UNIVERSITÉ DE SHERBROOKE

NSERC RESEARCH CHAIR IN FRP REINFORCEMENT FOR CONCRETE STRUCTURES

SERVICEABILITY OF CONCRETE BRIDGE DECK SLABS REINFORCED WITH FRP COMPOSITE BARS

TECHNICAL REPORT

Prepared by

El-Salakawy, E. and Benmokrane, B.

ISIS-Sherbrooke, Department of Civil Engineering,
Faculty of Engineering
University of Sherbrooke, Sherbrooke, Quebec, Canada J1K 2R1
Tel: (819) 821-7758
Fax: (819) 821-7974
E-mail: Brahim.Benmokrane@USherbrooke.ca

ISIS CANADA

The canadian Network of Centres of Excellence on Intelligent Sensing for Innovative Structures
Le réseau canadian de Centres d'excellence sur les innovations en structures avec système de détection integré

July 2003

Authors Biography

ACI member **Ehab El-Salakawy,** is a Research Associate Professor in the Department of Civil Engineering at the Université de Sherbrooke, Sherbrooke, Québec, Canada. He is a member of ACI Committee 445-3, punching shear, and ISIS Canada, Network of Centers of Excellence. His research interests include large-scale experimental testing and finite element modeling of reinforced concrete structures, construction, and rehabilitation of concrete structures reinforced with FRP composites. He has been involved in the design, construction, testing, and monitoring of several FRP-reinforced concrete bridges in North America.

ACI member **Brahim Benmokrane** is an NSERC Research Chair Professor in FRP Reinforcement for Concrete Structures in the Department of Civil Engineering at the Université de Sherbrooke, Sherbrooke, Québec, Canada. He is a project leader in ISIS Canada Network of Centers of Excellence on Intelligent Sensing for Innovative Structures. His research interests include the application and durability of advanced composite materials in civil engineering structures and structural health monitoring with fiber optic sensors. He has been involved in the design, construction, and monitoring of the first three bridges (Joffre, Wotton, and Magog-Highway 55 Nord Bridges) constructed in Quebec using FRP bars in their concrete deck slabs.

Paper submitted to ACI Structural Journal

ABSTRACT

The serviceability concerns, specially cracking and deflections usually govern the design of reinforced concrete flexural members reinforced with FRP bars. This research program was designed to investigate the flexural behaviour and serviceability performance of concrete deck slabs reinforced with different types of FRP composite bars. A total of 10 full size one-way concrete slabs were constructed and tested. The slabs were 3100-mm long ×1000-mm wide × 200-mm deep. The test parameters were the type and size of FRP reinforcing bars, and the reinforcement ratio. Five slabs were reinforced with glass FRP, three were reinforced with carbon FRP bars, and two control slabs were reinforced with conventional steel. The slabs were tested under four-point bending over a simply supported clear span of 2500 mm and a shear span of 1000 mm. The test results are reported in terms of deflection, crack width, strains in concrete and reinforcement, ultimate capacity, and mode of failure. Comparison with the predictions of CAN/CSA-S806-02, CAN/CSA-S6-00 Codes and ACI 440.1R-01 design guidelines is also presented. Test results showed that slabs with a carbon or glass FRP reinforcement ratio equivalent to the balanced reinforcement ratio satisfy serviceability and strength requirements of the considered design codes.

Table of Contents

Page

List of Tables

List of Figures

1. INTRODUCTION

Fiber reinforced polymer (FRP) bars are used as reinforcement for concrete structures such as bridges and parking garages in which the corrosion of steel reinforcement has typically led to significant deterioration and rehabilitation needs. Bridge deck slabs are one of the most bridge components vulnerable to deterioration because of direct exposure to environment, de-icing chemicals, and ever-increasing traffic loads. The non-corrosive nature of the FRP bars provides a potential for increased service life, economic, and environmental benefits. However, the relatively low modulus of FRP composites, especially glass FRP, compared to steel reduces the serviceability performance of the flexural members. Having the same ultimate capacity, FRP reinforced members will have larger deflections and crack widths than steel reinforced members. Accordingly, in most cases, serviceability requirements govern the design of FRP reinforced concrete members (Matthys and Taerwe 1995; Michaluk et al. 1998; Hassan et al. 1999; Alkhrdaji et al. 2000; Khanna et al. 2000).

Several codes and design guidelines for concrete structures reinforced with FRP composite bars have been recently published (CAN/CSA-S6-00 2000; ISIS-M03-01 2001; ACI 440.1R-01 2001; CAN/CSA-S806-02 2002). Based on these codes and design guidelines, several concrete bridges have been recently constructed in North America using FRP composite bars as reinforcement for the concrete deck slabs (Rizkalla and Tadros 1994; GangaRao et al. 1997; Steffen et al. 2001; El-Salakawy et al. 2003a; Benmokrane et al. 2003; El-Salakawy and Benmokrane 2003). In the constructed bridges, different FRP reinforcement types, ratios, and configurations were used based on flexural behaviour of the concrete deck slab and different serviceability criteria.

An extensive research program is being carried out at the Université de Sherbrooke to investigate and develop corrosion-free FRP-reinforced concrete bridges. Concrete bridge barriers was the first bridge component to be developed using glass FRP bent bars to connect the barrier wall to the concrete deck slab (El Salakawy et al. 2003b). The second bridge component, deck slabs, is currently under investigation for both flexural and shear behaviour. This paper presents the test results in terms of flexural behaviour and serviceability performance of one-way concrete bridge deck slabs reinforced with FRP composite bars compared to the available design models.

2. RESEARCH SIGNIFICANCE

Due to lower stiffness of FRP bars compared to steel, deflection and crack width can be the controlling parameters of design. Furthermore, with the recent publication of several codes and guidelines for design and constructions of concrete structures reinforced with FRP bars, the need to examine serviceability-related issues and validate/improve the accuracy of these guidelines is highly demanded. This paper investigates the serviceability performance of full size one-way bridge deck slabs reinforced with different types, ratios, and configurations of FRP bars.

3. EXPERIMENTAL PROGRAM

The balanced reinforcement ratio, ρ_b, of a concrete section is the reinforcement ratio at which a simultaneous rupture of FRP bars (yielding for steel) and crushing of concrete occur. The FRP-reinforced test slabs were designed such that the actual reinforcement ratio is equal to or greater than the balanced reinforcement ratio, ρ_{fb}, which is given in Section 8.2.1 of ACI 440.1R-01 (2001) as:

$$\rho_{fb} = 0.85\ \beta_1\ \frac{f_c^{'}}{f_{fu}}\frac{E_f \varepsilon_{cu}}{E_f \varepsilon_{cu} + f_{fu}} \qquad (1)$$

where $\beta_1 = 0.97 - 0.0025\ f'_c \geq 0.67$, f'_c is the compressive strength of concrete(MPa), f_{fu} is the ultimate tensile strength of FRP Bars (MPa), E_f is the modulus of elasticity of FRP bars (MPa), ε_{cu} is the maximum usable compressive strain in the concrete (assumed to be 0.003). The actual reinforcement ratios of the tested slabs were calculated assuming the effective depth of the slab to be the distance between the top of the slab and the centroid of the lower reinforcement in the main (considered) direction, which is suitable for the analysis purposes. However, in reinforcement ratio calculation, the CAN/CSA-S6-00 (2000) Code considers the effective depth of the slab as the distance between the top of the slab and the centroid of the lower reinforcement assembly. Furthermore, due to the higher strength of FRP bars compared to the yield strength of steel, the balanced reinforcement ratio for slabs reinforced with FRP bars is very small (0.39% and 0.86% for carbon and glass FRP, respectively) compared to that of steel (4.6%).

3.1 Material Properties

The slabs were constructed using normal-weight ready-mixed concrete. Compressive tests carried out on three 150 × 300 mm concrete cylinders, for each concrete batch, yielded an average compressive strength of 40 MPa after 28 days and a modulus of elasticity of 30 GPa. An average concrete tensile strength of 3.5 MPa was obtained by performing the split cylinder tests. Sand-coated glass and carbon FRP bars, with a fiber content of 73% in a vinyl ester resin, were used. The mechanical properties of FRP bars were determined by performing tensile tests on FRP specimens (Benmokrane et al. 2002). The test results yielded an average ultimate tensile strength and modulus of 1536 MPa and 114 GPa for carbon FRP, 597 (540) MPa and 40 GPa for

glass FRP bars, respectively. Table 1 lists the mechanical characteristics of FRP and steel reinforcement used in reinforcing the tested slabs.

3.2 Test Specimens

A total of 10 full size slabs were constructed and tested to failure. The slabs were 3100-mm long ×1000-mm wide × 200 mm deep. These dimensions were chosen to represent the most common size of the concrete deck slabs for girder-type bridges in North America (Rizkalla and Tadros 1994; GangaRao et al. 1997; Steffen et al. 2001; E El-Salakawy et al. 2003a; Benmokrane et al. 2003; El-Salakawy and Benmokrane 2003). The test parameters were the type, size and ratio of FRP reinforcement in the main bottom direction.

The test slabs were divided into three series. Series I included two control slabs reinforced with conventional steel bars. The first control slab, S-ST1 (with a reinforcement ratio of 0.55 % using singly placed No.10M, 100 mm^2, steel bars), represented the required steel reinforcement according to the flexural design method in AASHTO (AASHTO 1996) and the CHBDC (CAN/CSA-S6-00 2000) Codes (see Figure 1). While the second control slab, S-ST2 (with a reinforcement ratio of 0.86 % using singly placed No.15M, 200 mm^2, steel bars), represented what is commonly used by most departments of transportation in North America.

Series II included three slabs reinforced with carbon FRP bars, S-C1, S-C2B, and S-C3B. FRP carbon bars No.10 (d_b = 9.5 mm, A_b = 71 mm^2) were used with three configurations, singly placed, two bundled, and three bundled bars corresponding to three reinforcement ratios equal to ρ_b, $2\rho_b$, and $3\rho_b$, respectively. Series III included five slabs reinforced with glass FRP bars, S-

G1, S-G2, S-G2B, S-G3, and S-G3B. FRP glass bars No.16 (d_b = 15.9 mm, A_b = 198 mm^2) were used for slabs S-G1, S-G2B, and S-G3B with three configurations identical to those of series II slabs. To investigate the effect of bar diameter, two slabs, S-G2 and S-G3 were reinforced, using No.22 (d_b = 22.2 mm, A_b = 387 mm^2) glass FRP reinforcing bars, with the same reinforcement ratios and bar spacing as S-G2B and S-G3B, respectively, were also constructed and tested.

All tested slabs have identical glass FRP reinforcement in all directions except the bottom reinforcement in the main direction and a clear concrete cover of 50 and 30 mm at top and bottom, respectively as shown in Figure 2a. Although, these slabs were tested in one position (between girders), they represent the flexural behaviour of a real deck slab at the two critical locations, between and above girders, where the design moment is the same.

It should be noted that in common practice, a membrane layer along with a top concrete cover of 50-75 mm are used to delay corrosion of steel reinforcement, which have the disadvantages of adding extra weight and having larger crack widths. However, for the non-corrosive FRP bars, there is no need for either the thick concrete cover or the membrane layer. This was implemented in the CHBDC (CAN/CSA-S6-00) by reducing the allowable minimum top and bottom concrete cover in deck slabs to 35± 10 mm when using FRP composites.

Table 2 lists the reinforcement details of the test slabs. The axial stiffness of the FRP reinforcement, $E_f A_f$, as a ratio of that of the steel reinforcement, $E_s A_s$, (slab S-ST1) for all slabs is also listed in this Table 2. This ratio has a direct relationship with the expected values of maximum deflections and crack widths for the FRP-reinforced slabs compared to the reference

slab S-ST1. Slabs with similar $E_f A_f$, / $E_s A_s$ ratio would have similar values of deflections and crack widths.

3.3 Instrumentation

Electrical resistance strain gauges were glued on reinforcing bars and on concrete surface, at mid-span to measure strains during testing. The mid-span deflection was measured using two Linear Variable Differential Transformers (LVDTs) located at each side of the slab. After cracking, two high-accuracy LVDTs (± 0.001 mm) were installed at the positions of the first two cracks to measure the largest crack widths.

3.4 Test Set-up and Procedure

The slabs were tested under four-point bending over a clear span of 2500 mm and a shear span of 1000 mm, as shown in Figure 2. The load was statically applied at a stroke-controlled rate of 1.2 mm/min to achieve failure in 25 to 55 minutes. The loading was stopped when the first two cracks appeared and the initial crack widths were measured manually using a 50X hand-held microscope. Then the two high-accuracy LVDTs were installed to measure crack width electronically with increasing load. The larger value of the two measured crack widths was considered in the analysis. During loading, the formation of cracks on the sides of the slabs were also marked and recorded.

4. TEST RESULTS AND DISCUSSION

According to AASHTO (AASHTO 1996) and the Canadian Highway Bridge Design Code (CAN/CSA-S6-00 2000), a concrete deck slab of 200 mm thickness is required for a slab-on-

girder type bridge with a centerline-to-centerline spacing of approximately 1.8 to 2.5 m between girders. Also, it is proposed to design the concrete deck, based on flexural behaviour, for dead loads and live wheel loads plus impact (see Figure 1). This approach yields service, M_{ser}, and ultimate, M_{ult}, design moments of approximately 30 to 35 kN.m/m and 50 to 60 kN.m/m, respectively, at top and bottom in the deck slab except at the overhang where higher values are expected (El-Salakawy and Benmokrane 2003; see also the Appendix A: Design Example). In the following discussion, to define a reference for comparison purposes, the service and ultimate load levels, M_{ser} and M_{ult}, of the tested slabs were considered as 35 kN.m (1.4 M_{cr}) and 60 kN.m (2.4 M_{cr}), respectively (M_{cr}, is calculated based on concrete compressive strength of 40 MPa). This value of M_{ser} is at least 30% greater than the value obtained using finite element analysis (Massicotte, B., personal communication). The test results will focus on deflections and cracking. However, strains in FRP bars and concrete, ultimate capacity, and mode of failure will be also presented.

4.1 Deflection Characteristics

Figure 3 shows the mid-span deflection versus applied moment for the tested slabs. For FRP reinforced slabs, the load-deflection curve is bilinear. The first part up to the cracking moment (M_{cr} = 23 to 24 kN.m) was similar to the control slabs representing the behaviour of the uncracked slab utilizing the gross inertia of the concrete cross-section, while the second part represents the cracked slab with reduced inertia. For steel reinforced slabs, S-ST1 and S-ST2, the load-deflection curve is tri-linear with yielding plateau.

It should be noted that the observed experimental cracking moments (23 to 24 kN.m) did not include the moment due to the own weight of the slabs (3.67 kN.m). Considering this value,

both observed and theoretical (25.3 kN.m, based on $f_t = 0.6 \sqrt{f_c'}$ MPa) cracking moments are very close.

The measured deflections, at service load level (35 kN.m), for the tested slabs are listed in Table 3. At service load level, the measured deflection for carbon FRP-reinforced slabs ranged between 3.7 mm (S-C3B) and 6.3 mm (S-C1) with a deflection over a span ratio of 1/675 to 1/400. While, for slabs reinforced with glass FRP bars, these values ranged between 4.6 mm (S-G3B) and 6.5 mm (S-G1) with a deflection over a span ratio of 1/540 to 1/385. The deflection behaviour of the two slabs S-G2 and S-G3, reinforced with No. 22 GFRP bars, was very similar to their counterparts S-G2B, and S-G3B reinforced with No.16 GFRP bars. In addition, the measured deflection at service load level for the second control slab, S-ST2, was 3.3 mm, which is 70% of that measured for S-ST1 (4.7 mm). It can be seen that the flexural stiffness of the slabs reinforced with FRP bars (both carbon and glass) increases with the increase of the reinforcement ratio. As expected, slabs reinforced with FRP bars with reinforcement stiffness ($E_f A_f$) close to that of the control slabs ($E_s A_s$) had very similar deflection behaviour to each other and to the control slab before yielding. The three slabs, S-C2B (carbon FRP bars) and S-G3B/S-G3 (glass FRP bars) compared to the control slab S-ST1, and Slab S-C3B (carbon FRP bars) compared to the control slab S-ST2 had very similar deflection behaviour.

It should be noted that due to continuity of the slab over girders in actual bridge deck, the deflections at the same load level are expected to be less than what were measured in the laboratory.

4.2 Cracking

Cracking patterns of some of the tested slabs at the two design load levels: service load level (1.4 M_{cr} = 35.0 kN.m), and ultimate load level (2.4 M_{cr} = 60 kN.m) are shown in Figure 4. Cracks in the flexural span were vertical cracks perpendicular to the direction of the maximum principal stress induced by pure moment. Cracking outside the pure bending zone started similarly to flexural cracks, but as the load was increased, shear stress become more dominant and induced inclined cracks. For all slabs, crack formation was initiated at a moment, M_{cr}, of 23 to 24 kN.m.

Table 3 lists the measured first crack widths and cracking characteristics at the service load level. The spacing between cracks decreased with increased reinforcement ratio. For the same bar spacing and size, increasing the FRP reinforcement ratio by 100 to 200% decreased the crack spacing by 44 to 49% and 4 to 10% for slabs reinforced with glass and carbon FRP bars, respectively. In addition, increasing the reinforcement ratio by 100% to 200% decreases the crack penetration depth by 11 to 36% and 15 to 22% for slabs reinforced with carbon and glass FRP bars, respectively.

Figure 5 shows the variation of the measured crack width against the applied moment for the tested slabs. For slab reinforced with FRP bars, the crack width varies linearly with the load up to failure and the initial cracking moment, M_{cr}, was approximately 23 to 24 kN.m. At service load level, the measured crack width for carbon FRP-reinforced slabs ranged between 0.12 mm (S-C3B) and 0.28 mm (S-C1). While, for slabs reinforced with glass FRP bars, these values ranged between 0.17 mm (S-G3) and 0.35 mm (S-G1). Thus increasing the FRP reinforcement ratio by 100% and 200% for slabs reinforced with carbon FRP bars, S-C2B and S-C3B,

decreased the crack widths by 41% and 57%, respectively. For slabs reinforced with glass FRP bars, S-G2B and S-G3B, these decreases in crack widths were 39% and 49%, respectively. These measured crack widths for FRP-reinforced slabs were well below the allowable code limit of 0.5 mm (ACI 440.1R-01 2001).

It should be noted that for the three slabs S-C2B and S-G3B/S-G3, with approximately similar flexural stiffness to the control slab S-ST1 (80 and 90 %, respectively), the total number of cracks, the average crack spacing, crack penetration depth, and crack width were quite similar to that of the control slab S-ST1. The same observation is valid for slabs S-C3B (carbon FRP bars) and S-ST2.

For slab S-G2, the effect of using larger bar size (No.22 GFRP bars) than S-G2B (No.16 GFRP bars) was decreasing the crack spacing and increasing the crack width and penetration depth. However, for slab S-G3 (No.22 GFRP bars), the effect of decreasing the bar spacing was dominant causing an increase in crack spacing and decrease in the crack width and penetration depth compared to slab S-G3B. Furthermore, the maximum measured crack width at service load level for the second control slab, S-ST2, was 0.11 mm, which is 65% of that measured for S-ST1 (0.17 mm).

4.3 Ultimate Capacity and Mode of Failure

All slabs reinforced with FRP bars failed in shear while the control steel-reinforced slabs, S-ST1 and S-ST2, failed by steel yielding followed by crushing of concrete. The two slabs reinforced with a reinforcement ratio equivalent to the balanced reinforcement ratio, S-G1 and S-C1, failed by tension-shear failure in the vicinity of the support showing an increase of the

capacity of only 26% and 55%, respectively compared to the control slab, S-ST1. This was due to the high strains developed in the reinforcing bars at failure, which increased the penetration depth and width of the shear crack and reduced the aggregate interlock as well as the area of concrete in compression that can resist shear.

For the six slabs reinforced with FRP reinforcement ratios higher than the balanced reinforcement ratio failed by compression-shear failure in the vicinity of the concentrated load showing an increase of the capacity of 81 to 111% compared to the control slab, S-ST1. This increase in carrying capacity may be due to increasing the contribution of the dowel action and the aggregate interlock to the shear strength of the slabs. Figure 7 shows photos of the two types of shear failures.

4.4 Strains in Reinforcement and Concrete

Figure 6 shows the measured mid-span strains in reinforcement as well as in concrete versus the applied moment. For the eight slabs reinforced with FRP bars, it can be noted that, after cracking, the strains vary linearly with the increased load up to failure and the maximum measured strains were less than the ultimate strains of the FRP materials. Also, the increase in FRP reinforcement ratio decreased the strains measured in both bars and concrete. The measured strains in the FRP bars of the two slabs reinforced with a reinforcement ratio equivalent to the balanced reinforcement ratio, S-G1 and S-C1 were approximately 13000 micro-strain and 11000 micro-strain, respectively, which are close to the ultimate strains of the FRP materials. The corresponding compressive strains in concrete for these two slabs were 3100 and 3000 micro-strain, respectively. However for the remaining over-reinforced slabs with FRP bars, the measured strains at ultimate ranged between 6000 to 8500 micro-strain and between 7000 to

10000 micro-strain for carbon and glass FRP bars, respectively. For these six slabs, the maximum compressive strains in concrete were 2000 to 2600 micro-strain.

For the control slabs reinforced with steel (S-ST1 and S-ST2), a typical steel-yielding plateau was obtained with a maximum measured strain of approximately 12000 micro-strains. After steel yielding, the compression strains in concrete increased resulting in failure by concrete crushing.

5. CODE PREDICTIONS

5.1 Deflections

Most code provisions for deflection control of cracked one-way reinforced concrete flexural members depend on the section effective moment of inertia, I_e, which is inserted into elastic deflection equations instead of the gross moment of inertia. Due to the difference in stiffness and bond characteristics between FRP and steel bars, the following expression is given by the ACI 440.1R-01 (2001) guidelines:

$$I_e = \left(\frac{M_{cr}}{M_a}\right)^3 \beta_d I_g + \left[1 - \left(\frac{M_{cr}}{M_a}\right)^3\right] I_{cr} \le I_g \text{ and } \beta_d = \alpha_b \left(\frac{E_f}{E_s} + 1\right) \qquad (2)$$

in which M_{cr} and M_a are the cracking and the applied moments, respectively, E_s, E_f are modulus of elasticity of steel and FRP bars (GPa), respectively, I_{cr} and I_g are cracked and gross moments of inertia of concrete section (mm^2), respectively, and α_b is a bond-dependant coefficient, which

may be taken as 0.5. This value of α_b was based on tests carried out on beams reinforced with glass FRP bars (ACI 440.1R-01, 2001).

The Canadian Code (CAN/CSA-S806-02 2002) used the moment-area method to develop closed-form deflection equations for several common types of loading and support conditions. This method is based on the assumption that the moment-curvature relation of a cracked FRP reinforced member remains linear under increasing load with flexural rigidity of $E_c I_{cr}$, and that tension stiffening is negligible. For a one-way slab under two-point loading, the maximum deflection is given by:

$$\delta_{\max} = \frac{PL^3}{24E_c I_{cr}}\left[3\left(\frac{a}{L}\right) - 4\left(\frac{a}{L}\right)^3 - 8\eta\left(\frac{L_g}{L}\right)^3\right] \text{ and } \eta = \left(1 - \frac{I_{cr}}{I_g}\right) \qquad (3)$$

in which P is the applied load, L is the span of the slab, a is the shear span, and L_g is the distance from support to point where $M_a = M_{cr}$ in simply supported slabs.

The predicted deflections using both codes were in good agreement with the test as shown in Figure 8. However, the deflection predictions of the CSA code seem to be more conservative especially at low load levels.

5.2 Crack width

According to the current practice, the maximum crack width limitation is set for two reasons, corrosion of reinforcement and the aesthetic point of view. In both ACI (ACI 318-

02/318R-95 1995) and CSA (CSA A23.3-94 1994) codes, for steel-reinforced concrete structures this limit was set to 0.3 mm for exterior exposure and 0.4 mm for interior exposure. As the FRP usually has lower modulus of elasticity compared to steel, crack widths in FRP reinforced members are expected to be larger than those in steel-reinforced members. However, for the non-corrosive FRP reinforcement, if the primary reason for crack width limitation is the corrosion of reinforcement, this limitation can be relaxed. Thus, the CSA S6-96, ACI 440.1R-01, and CAN/CSA S806-02 increased the allowable crack width limits to 0.5 and 0.7 mm for exterior and interior exposure, respectively, when FRP reinforcement is used.

For steel-reinforced concrete flexural members (ACI 318-02/318R-95 1995 and CSA A23.3-94 1994), the crack width, *w*, is calculated based on Gergely-Lutz empirical equation:

$$w = 11\ \beta\ f_s \sqrt[3]{d_c A} \times 10^{-6}\ \text{(mm)} \qquad (4)$$

The ACI 440.1R-01 introduced an adjusted Gergely-Lutz equation to predict crack width, by multiplying equation 4 by two factors: E_s/E_f and k_b to get:

$$w = \frac{2.2}{E_f} \beta k_b f_f \sqrt[3]{d_c A} \quad \text{(mm)} \quad \text{considering } E_s = 200\,000 \text{ MPa} \qquad (5)$$

where A is effective tension area of concrete that surrounds the main tension reinforcement and has the same centroid as that reinforcement, divided by the number of bars (in mm^2); d_c is thickness of concrete cover measured from extreme tension fiber to the center of the nearest longitudinal bar (in mm); f_f is stress in reinforcement at specified load, calculated by elastic

cracked section theory (in MPa); $\beta = h_1/h_2$ where h_1 is distance from centroid of tension reinforcement to neutral axis (in mm) and h_2 is distance from extreme tension fiber to neutral axis (in mm); k_b is a bond-dependant coefficient that equals one, larger than one or smaller than one, for FRP bras having bond behaviour equal to, inferior to or superior to steel, respectively. A value of k_b, equals to 1.2 is recommended by ACI 440.1R-01. The ratios of experimental to predicted crack widths for the tested slabs assuming different values of k_b are listed in Table 4. Also, a comparison of experimental and predicted moment-crack width behaviour for specimens S-C2B and S-G3B is shown in Figure 9. In Table 4 and Figure 9, the ACI predictions are based on a reduced theoretical cracking moment value of 21.63 kN.m excluding the moment resulting from the own weight of the slab (3.67 kN.m). A k_b value of 1.0 seems to give better correlation with the test results yet conservative. Furthermore, assuming the same initial crack width, experimental and theoretical predictions will be nearly identical for a k_b value of 1.0.

For cracking control, the new Canadian Code (CAN/CSA-S806-02 2002) introduced a parameter, z, which is also based on equation 4.

$$z = \frac{E_s}{E_f} k_b f_f \sqrt[3]{d_c A} \qquad (6)$$

The parameter z should not exceed 45 000 N/mm for interior exposure and 38 000 N/mm for exterior exposure when FRP reinforcement is used.

Similar expression was introduced in the new Canadian Highway Bridge Design Code (CAN/CSA-S6-00 2000) for steel-reinforced flexural concrete elements. As given in this code, replacing steel with FRP bars of the same axial stiffness automatically satisfies cracking allowable limits for FRP-reinforced members.

It should be noted that at service load level, the measured crack widths and control parameters for all tested slabs were well below the allowable specified limits of 0.5 mm (CSA S6-96; ACI 440.1R-01; CAN/CSA S806-02) and 38 000 N/mm (CAN/CSA-S806-02 2002), respectively.

6. DUCTILITY AND DEFORMABILITY

Ductility of a reinforced concrete element provides a measure of the energy absorption capability. Ductility of concrete members reinforced with steel bars is defined as the ratio of deflection or curvature values at ultimate to those at yielding of steel. As there is no yielding point for FRP composite bars, a parameter for comparing the ductility behaviour of FRP-reinforced beams with that of steel-reinforced ones has been developed by Jaeger et al. and it is referred to as J-factor or deformability factor (Jaeger et al. 1995). The factor is calculated as the product of the ratio of the moment at ultimate, M_{ult}, to the moment at a certain service condition, M_c, called the strength factor, and the ratio of the curvature at ultimate, $\psi_{ult,}$ to curvature at the same service condition, $\psi_{c,}$ called the curvature factor.

$$J = \frac{M_{ult}}{M_c} \times \frac{\psi_{ult}}{\psi_c} \qquad (7)$$

The service condition is defined as the upper limit of elastic behaviour of concrete, which was taken corresponding to ε_c = 0.001. This approach is adopted by the Canadian Highway Bridge Design Code (CSA-S6-00 2000), which requires a J-factor exceeding 4 for rectangular sections. Table 3 lists the values of the deformability factor using the above approach. For all

tested slabs, the J-factor is well above the CSA-S6-00 (2000) Code limit of 4 (for rectangular sections). The higher the J-factor values the more ample warning the FRP-reinforced concrete member gives before failure. In other words, the J-factor indicates the amount of cracks and deflections of the FRP-reinforced concrete member will exhibit through load history from service to ultimate conditions.

7. CONCLUSIONS

A total of 10 full size one-way concrete slabs measuring 3100 ×1000 × 200 mm were constructed and tested under four point bending to failure. The test parameters were the type and size of FRP reinforcing bars, and the reinforcement ratio. Five slabs were reinforced with glass FRP, three were reinforced with carbon FRP bars, and two control slabs were reinforced with conventional steel. Due to the high strength of FRP bars, the strength of the FRP-reinforced slabs is not of a major concern and the test results were analyzed based on serviceability criteria (crack width and deflection). Based on the experimental test results, the following conclusions can be drawn:

(a) The carrying capacity of concrete slabs reinforced with composite FRP bars (carbon and glass) was much higher than the control slab reinforced with steel (26% to 111%). In addition, the FRP reinforced slabs failed by shear while the control slab failed by steel yielding followed by concrete crushing. Due to the high strength of the FRPs, this shear mode of failure occurred at a high load that is not likely to reach in the field.

(b) The flexural stiffness of the slabs reinforced with FRP composite bars increased with the increase of the reinforcement ratio. The slabs S-G3B/S-G3 (glass FRP - 2.5%) and S-C2B (carbon FRP - 0.78%) have very similar flexural behaviour to the control slab, S-ST1

reinforced with steel (0.55%). Same conclusion is valid for slabs S-C3B (carbon FRP - 1.18%) and S-ST2 (steel - 0.86%)

(c) In Slabs, S-G2B and S-G2 (with the same FRP reinforcement ratio), different bar sizes (No.16 and No.22), placed at the same spacing, has no significant effect on the flexural behaviour of the two slabs.

(d) In Slabs, S-G3B and S-G3 (with the same FRP reinforcement ratio), decreasing bar spacing (from 150 to 100 mm) improved cracking characteristics. However, it has no significant effect on deflection or ultimate capacity.

(e) The values of the deformability factor, J, for the 8 concrete slabs reinforced with composite material reinforcement were well above the limit required by the Canadian Highway Bridge design Code (CSA-S6-00 2000).

(f) Deflections predicted by both codes were in good agreement with the test results. However, the deflection predictions of the CSA code seem to be more conservative especially at low load levels.

(g) For crack width prediction by ACI 440.1R-01, a k_b value of 1.0 seems to give better correlation with the test results yet conservative.

All tested FRP-reinforced concrete slabs satisfied the serviceability allowable limits in terms of crack width and deflection.

8. RECOMMENDATION

Based on the presented laboratory tests and the results of field tests (El-Salakawy and Benmokrane 2003), for concrete bridge deck slabs supported on girders and have span-to-depth ratio less than 15, the following FRP reinforcement configuration in the transverse direction is recommended:

- Glass FRP bars No.15 @ 150 mm (top and/or bottom)
- Carbon FRP bars No.10 @ 110 mm (bottom)

To facilitate construction and resist stresses resulting from shrinkage and temperature changes, glass FRP bars No. 15 @ 150 mm can be used in the longitudinal direction at top and bottom. This is valid for carbon and glass FRP composite bars with a modulus of elasticity of at least 110 and 40 GPa, respectively, with a concrete cover of 40 mm top and bottom. This bridge deck slab design is adequate in terms of structural performance, safety, durability, and economy.

ACKNOWLEDGEMENT

The authors thank the Ministry for Transport of Quebec (Department of Structures - Québec City, Québec) and Pultrall Inc (Thetford Mines, Québec). The partial finance received from the Natural Science and Engineering Research Council of Canada (NSERC) and the Network of Centres of Excellence ISIS-Canada is greatly appreciated. The authors would like to thank François Ntacorigira and Simon Sindayiagaya, technicians at Civil Engineering Department, Université de Sherbrooke for their help.

REFERENCES

1. AASHTO, (1996), "Standard Specifications for Design of Highway Bridges", American Association of State Highway and Transportation Officials, Washington, DC.
2. ACI 318-02/318R-95, (1995), "Building Code Requirements for Structural Concrete and Commentary", American Concrete Institute, Farmington Hills, Michigan, 391p.
3. ACI 440.1R-01, (2001) Guide for the Design and Construction of Concrete Reinforced with FRP Bars, American Concrete Institute, Farmington Hills, Michigan, 41p.
4. Alkhrdaji, T., Ombres, L., and Nanni, A., (2000), "Flexural Behaviour of One-way Concrete Slabs Reinforced with Deformed GFRP Bars", Proceedings of the 3rd Conference on Advanced Composite Materials in Bridges and Structures, Ottawa, pp. 217-224.
5. Benmokrane, B., Zhang, B., Laoubi, K., Tighiouart, B., and Lord, I., (2002), "Mechanical and Bond Properties of New Generation of CFRP Reinforcing Bars for Concrete Structures", Canadian Journal of Civil Engineering, Vol. 29, No. 2, pp.338-343.
6. Benmokrane, B., El-Salakawy, E. F., Nadeau, D., and Lackey, T., (2003), "Building a New Generation of Concrete Bridge Decks using Innovative FRP Composite Bars", submitted, ACI Concrete International Magazine, American Concrete Institute, Farmington Hills, Michigan, 12p.
7. CAN/CSA-S6-96, (1996), "Canadian Highway Bridge Design Code", Canadian Standard Association, Rexdale, Ontario, Canada, 190 p.
8. CAN/CSA-S6-00, (2000), "Canadian Highway Bridge Design Code", Canadian Standard Association, Rexdale, Ontario, Canada, 192 p.
9. CSA A23.3-94, (1994). "Design of Concrete Structures for Buildings," Canadian Standards Association, Rexdale, Toronto, Ontario, 220 p.

10. CSA S806–02, (2002), "Design and Construction of Building Components with Fibre Reinforced Polymers", Canadian Standards Association, Rexdale, Ontario, 177 P.
11. El-Salakawy, E. F. and Benmokrane, B., (2003), "Design and Testing of a Highway Concrete Bridge Deck Reinforced with Glass and Carbon FRP Bars", in print, ACI Special Publication, FRP Composites for Internal Reinforcement, American Concrete Institute, Farmington Hills, Michigan, 25p.
12. El-Salakawy, E. F., Benmokrane, B., Desgagné, G., (2003a), "FRP Composite Bars for the Concrete Deck Slab of Wotton Bridge", in Print, Canadian Journal of Civil Engineering, 32p.
13. El-Salakawy, E. F., Benmokrane, B., Briére, F., Masmoudi, R., and Beaumier, E., (2003b), "Concrete Bridge Barriers Reinforced with GFRP Composite Bars," in print, ACI Structural Journal.
14. GangaRao, H.V.S., Thippesway, H.K., Kumar, S. V., and Franco, J.M., (1997), "Design, Construction and Monitoring of the First FRP Reinforced Concrete Bridge Deck in the United States", Proceedings of the 3rd International Symposium (FRPRCS-3) on Non-Metallic (FRP) Reinforcement for Concrete Structures, Sapporo, Japan, Vol. 1, pp. 647-656.
15. Hassan, T., Rizkalla, S., Abdelrahman, A., and Tadros, G., (1999), "Design Recommendations for Bridge Deck Slabs Reinforced by Fiber Reinforced Polymers", Proceedings of the Fourth International Symposium on Fiber Reinforced Polymers Reinforcement for Concrete Structures, FRPRCS-4, ACI-SP-188, Baltimore, USA, pp.313-323.
16. ISIS-M03-01, (2001), "Reinforcing Concrete Structures with Fibre Reinforced Polymers", The Canadian Network of Centers of Excellence on Intelligent Sensing for Innovative Structures, ISIS Canada, University of Winnipeg, Manitoba, 81 p.

17. Jaeger, G.L., Tadros, G., and Mufti, A.A., (1995), "Balanced Section, Ductility and Deformability in Concrete with FRP Reinforcement", Research Report No. 2-1995, Industry Center for Computer-Aided Engineering, Technical University of Nova Scotia (Now Dalehousie University), Halifax, NS, Canada, 29 p.
18. Khanna, S., Mufti, A., and Bakht, B., (2000), "Experimental Investigation of the Role of Reinforcement in the Strength of Concrete Deck Slabs", Canadian Journal of Civil Engineering, Vol. 27, No. 5, pp.475-480.
19. Massicotte, B., Department of Civil Engineering , Ecole Polytechnique de Montreal, Quebec, Canada.
20. Matthys, S. and Taerwe, L., (1995), "Loading tests on Concrete Slabs Reinforced with FRP Grids," Proceedings, The Second International Symposium: Non-metallic (FRP) Reinforcement for Concrete Structures, Taerwe, L. ed., Ghent, Belgium, August, pp.287-297.
21. Michaluk, R., Rizkalla, S., Tadros, G., and Benmokrane B., (1998), "Flexural Behaviour of One-way Concrete Slabs Reinforced with Fibre Reinforced Plastic Reinforcements," ACI Structural Journal, Vol. 95, No. 3, pp. 145-157.
22. Rizkalla, S., and Tadros, G., (1994), "First Smart Bridge in Canada", ACI Concrete International, Vol. 16, No. 6, pp. 42-44.
23. Steffen, R.E., Trunfio, J.P., and Bowman, M.M., (2001), "Performance of a Bridge Deck Reinforced with CFRP Grids in Rollinsford, New Hampshire, USA", Proceedings, FRP Composites in Constructions, Porto, Portugal, pp. 671-676.

Table 1. Properties of reinforcing bars

Bar Type	Diameter (mm)	Area (mm^2)	Modulus of Elasticity (GPa)	Tensile Strength (MPa)	Ultimate Strain (%)
CFRP	9.50	71	114 ± 2	1536 ± 31	1.20 ± 0.0
GFRP	15.90	198	40 ± 1	597 ± 36	1.49 ± 0.1
	22.20	387	40 ± 1	540 ± 33	1.35 ± 0.1
STEEL	11.30	100	200	f_y = 460	ε_y = 0.2
	15.96	200	200	f_y = 460	ε_y = 0.2

Table 2. Details of slab reinforcement in the bottom main direction

Slab		ρ_{act} (%)	$\frac{\rho_{act}}{\rho_b}$ * (%)	$\frac{E_f A_f}{E_s A_s}$ +	*Reinforcement configuration*	*Total No. of bars*
Series I Steel	S-ST1	0.55	0.12	1.0	No.10M @110 mm	9
	S-ST2	0.86	0.19	1.57	No.15M @150 mm	7
Series II Carbon	S-C1	0.39	1.0	0.40	No.10 @110 mm	9
	S-C2B	0.78	2.0	0.80	2 No.10 @110 mm	18
	S-C3B	1.18	3.0	1.20	3 No.10 @110 mm	27
Series III Glass	S-G1	0.86	1.0	0.30	No.16 @150 mm	7
	S-G2	1.70	2.0	0.60	No.22 @150 mm	7
	S-G2B	1.71	2.0	0.60	2 No.16 @150 mm	14
	S-G3	2.44	3.0	0.90	No.22 @100 mm	10
	S-G3B	2.63	3.1	0.92	3 No.16 @150 mm	21

* ρ_{act}, ρ_b = the actual and balanced reinforcement ratio, respectively

+ Considering slab S-ST1 as reference

Table 3. Summary of test results

Slab		Moment at failure (kN.m)	Deflection at service (mm)	1st crack width (mm)	Max. crack width (mm)		Crack depth (mm)		Crack spacing (mm)		No. of cracks		Deform-ability Factor	Failure Mode*
					$1.4M_{cr}$	$2.4M_{cr}$	$1.4M_{cr}$	$2.4M_{cr}$	$1.4M_{cr}$	$2.4M_{cr}$	$1.4M_{cr}$	$2.4M_{cr}$		
Series I	S-ST1	90	4.7	0.08	0.17	0.316	99	159	120	93	5	13	N/A	Y
	S-ST2	118	3.3	0.07	0.11	0.240	75	140	150	112	4	11	N/A	Y
Series II	S-C1	140	6.3	0.15	0.28	0.520	127	178	96	80	6	17	5.19	S
	S-C2B	167	4.8	0.09	0.17	0.321	100	155	115	90	5	15	6.00	S
	S-C3B	190	3.7	0.07	0.12	0.238	90	133	122	99	3	11	6.22	S
Series III	S-G1	113	6.5	0.20	0.35	0.690	132	159	88	75	8	17	5.95	S
	S-G2	142	5.6	0.12	0.24	0.447	121	153	92	82	6	15	6.75	S
	S-G2B	163	5.5	0.12	0.21	0.425	109	150	95	86	6	13	6.95	S
	S-G3	163	4.7	0.08	0.17	0.341	99	145	120	94	5	12	6.39	S
	S-G3B	168	4.6	0.08	0.18	0.339	97	143	118	94	5	12	6.61	S

* S = shear failure, Y = steel yielding

Table 4. Comparison of predicted and measured crack widths for FRP reinforced slabs

Slab	Experimental M_{cr} (kN.m)	Ratio of measured to ACI predicted crack width at service		
		K_b = 0.8	K_b = 1.0	K_b = 1.2
S-ST1*	23	N/A	0.82	N/A
S-ST2*	24	N/A	0.68	N/A
S-C1	23	0.75	0.60	0.50
S-C2B	24	0.87	0.70	0.58
S-C3B	24	0.78	0.63	0.52
S-G1	23	0.60	0.48	0.40
S-G2	23	0.69	0.55	0.46
S-G2B	23	0.70	0.57	0.47
S-G3	23	0.81	0.65	0.54
S-G3B	23	0.68	0.54	0.45

* Based on equation (4)

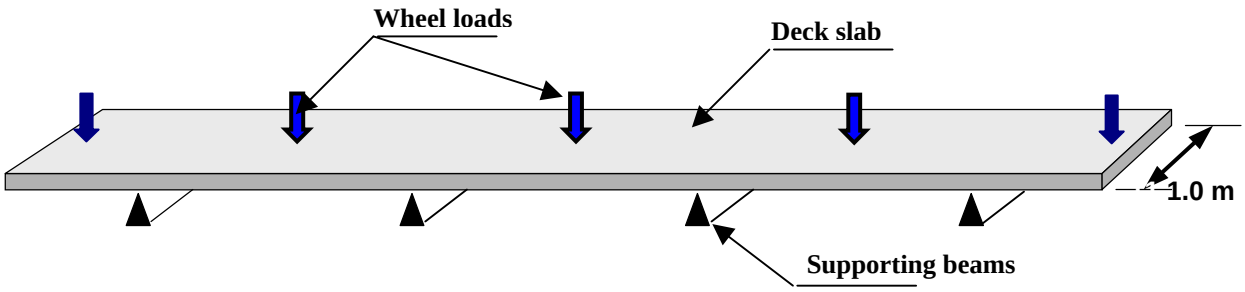

(a) Design strip of a bridge deck slab

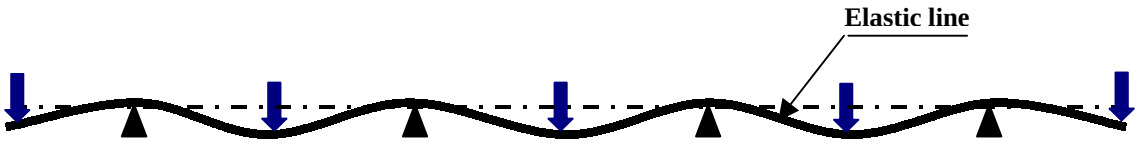

(b) Elastic line under concentrated wheel loads

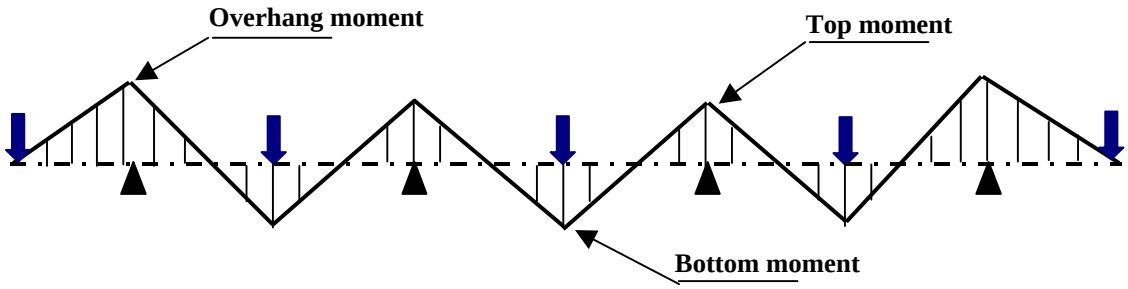

(c) Bending moment diagram

Figure 1. Assumed flexural behaviour of bridge deck slabs (AASHTO & CHBDC)

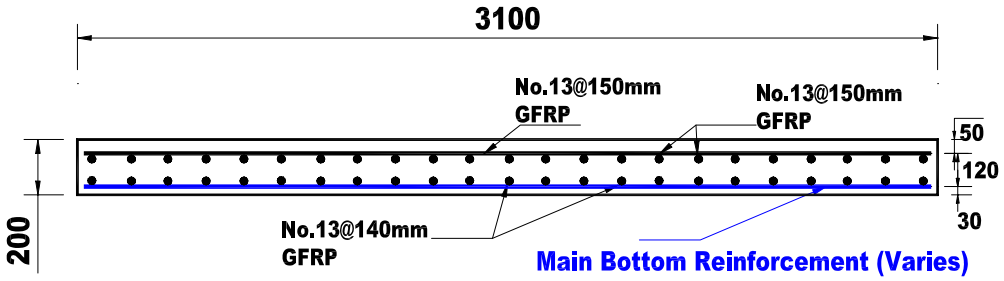

Clear cover: Top = 50 mm, Bottom = 30 mm

(a) Slab reinforcement

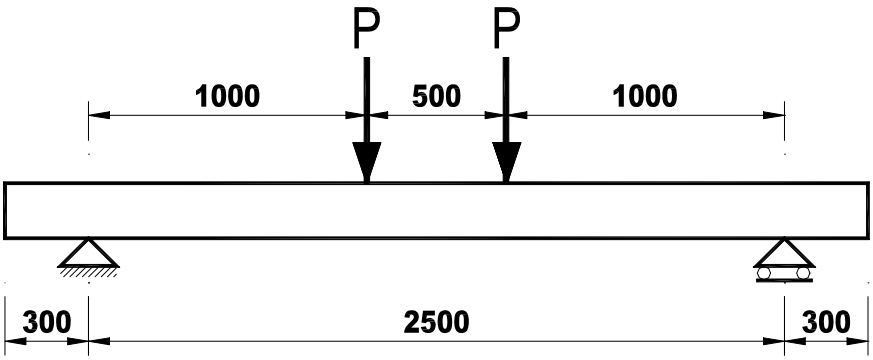

(b) Schematic drawing of the test set-up

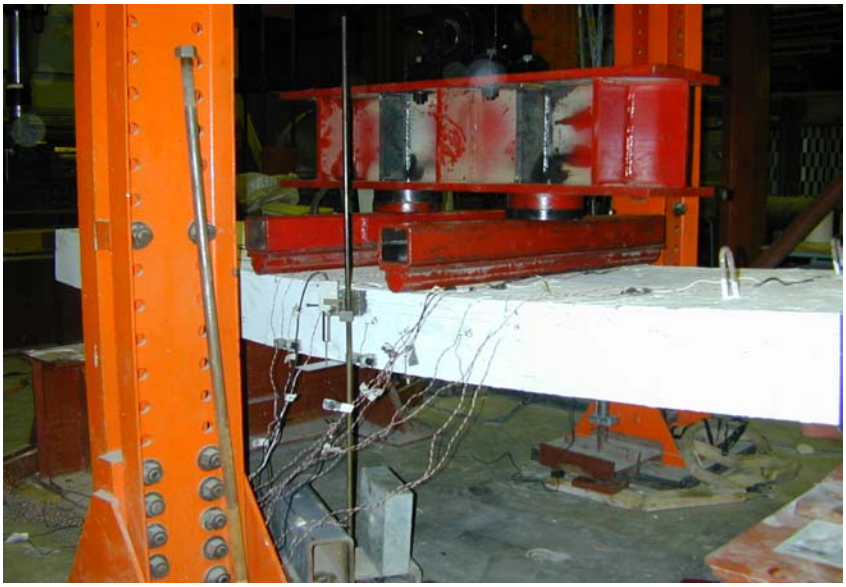

(c) Photo for test set-up

Figure 2. Test specimen and set-up

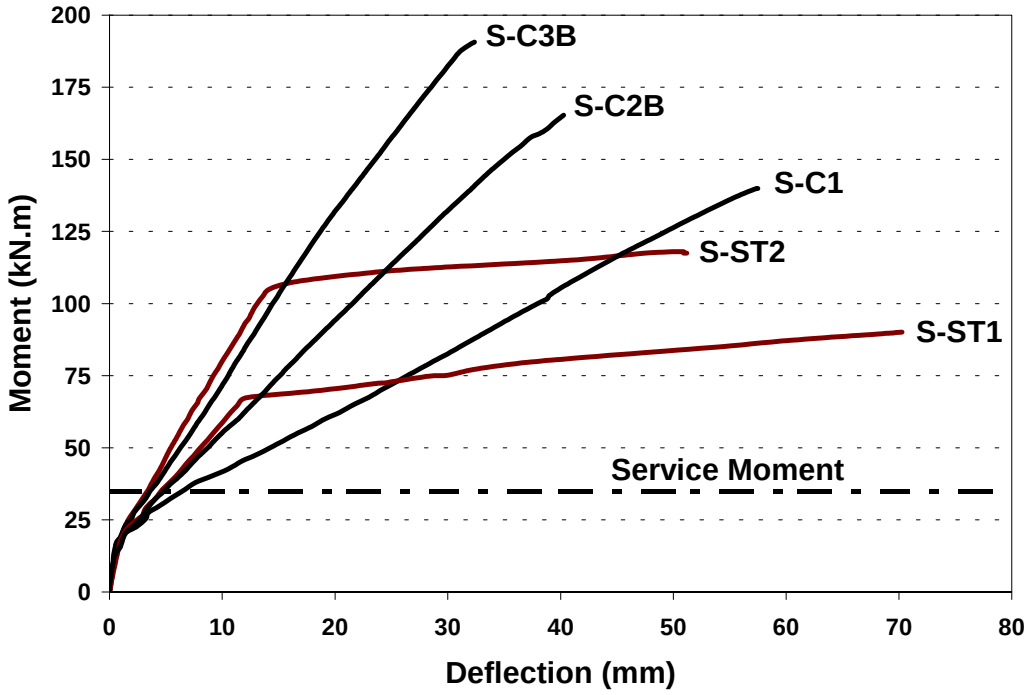

(a) Slabs reinforced with carbon FRP bars and the two controls

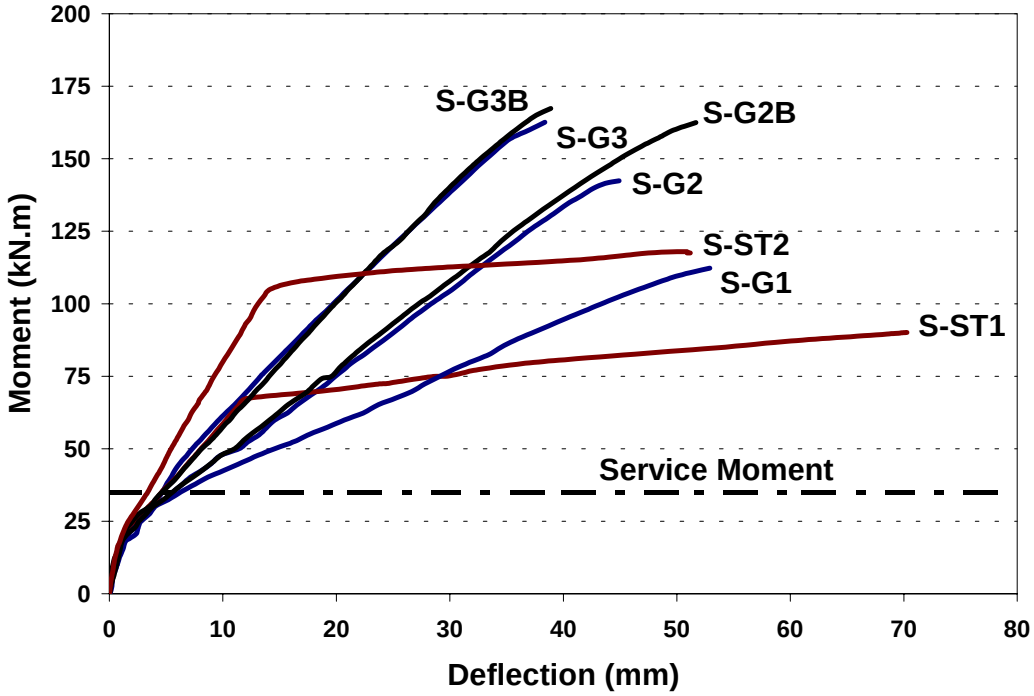

(b) Slabs reinforced with glass FRP bars and one control

Figure 3. Moment-deflection relationship for the tested slabs

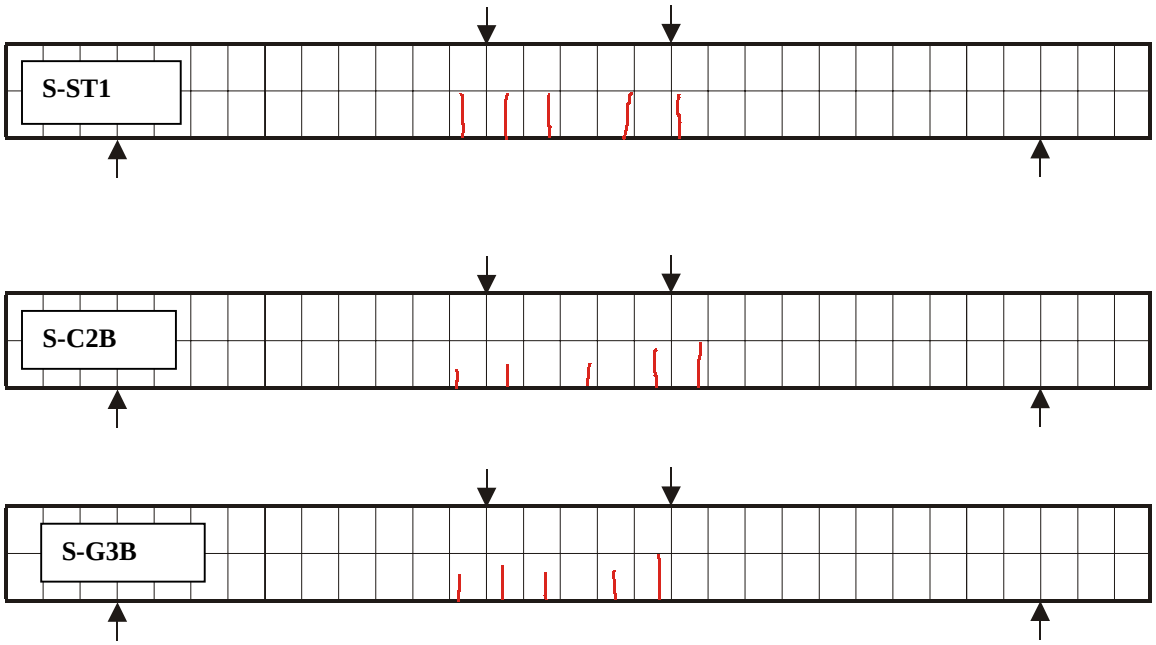

(a) At design service load level (1.4 M_{cr})

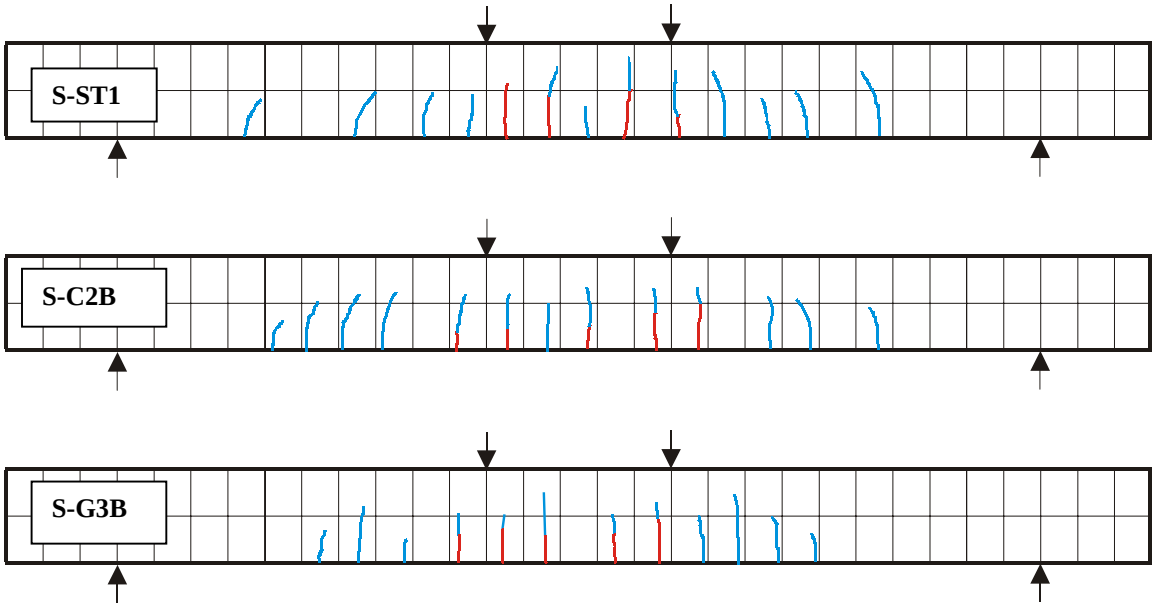

(b) At design ultimate load level (2.4 M_{cr})

Figure 4. Cracks pattern for selected slabs

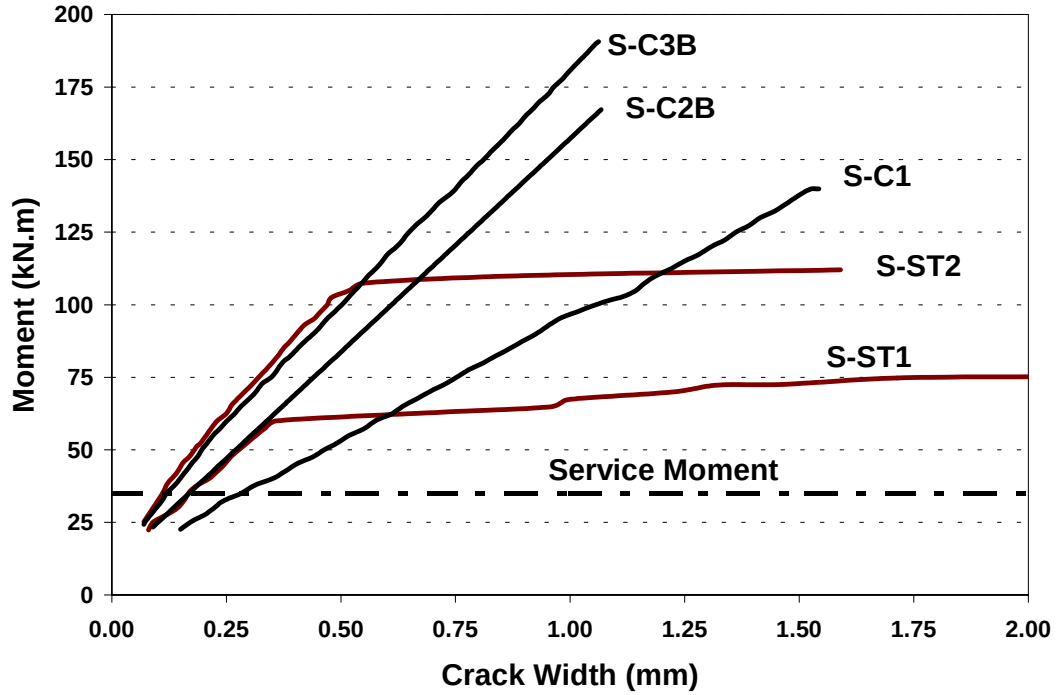

(a) Slabs reinforced with carbon FRP bars and the two controls

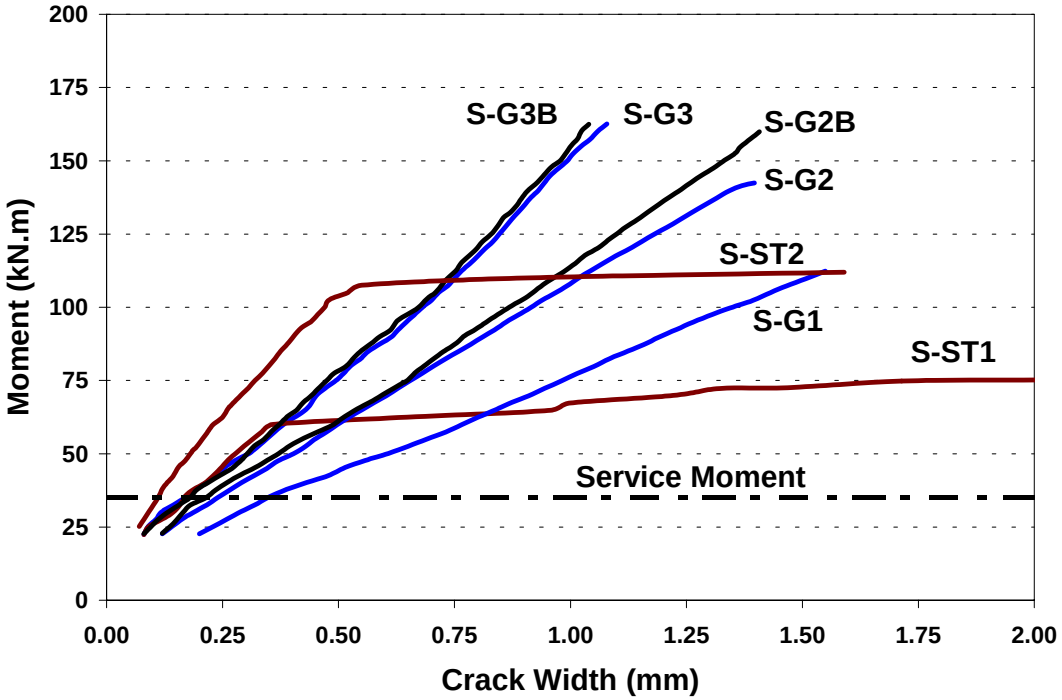

(b) Slabs reinforced with glass FRP bars and one control

Figure 5. Moment-crack width relationship

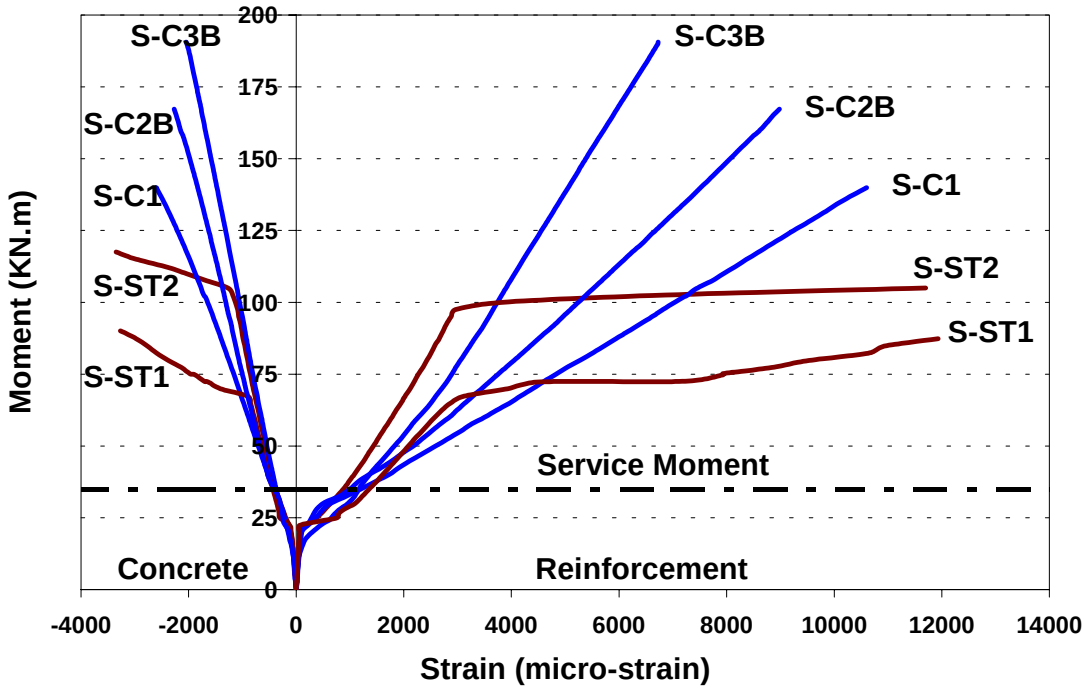

(a) Slabs reinforced with carbon FRP bars and the two controls

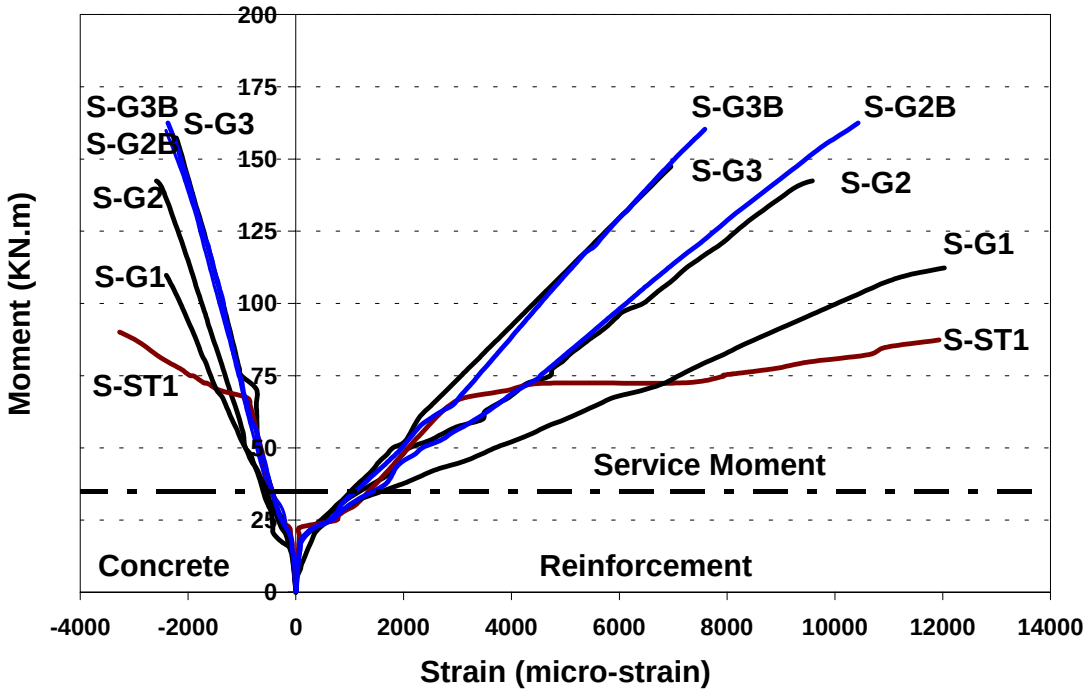

(b) Slabs reinforced with glass FRP bars and one control

Figure 6. Moment-strain relationship

(a) Tension-shear failure (S-C1)

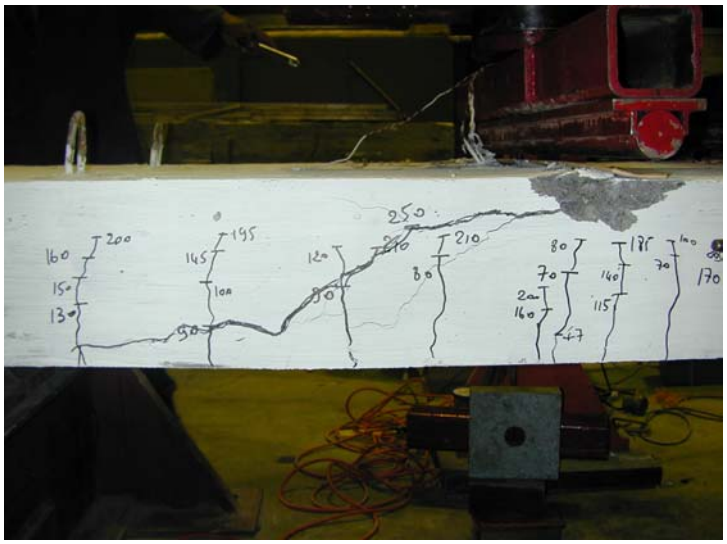

(b) Compression-shear failure (S-C2B)

Figure 7. Mode of failure

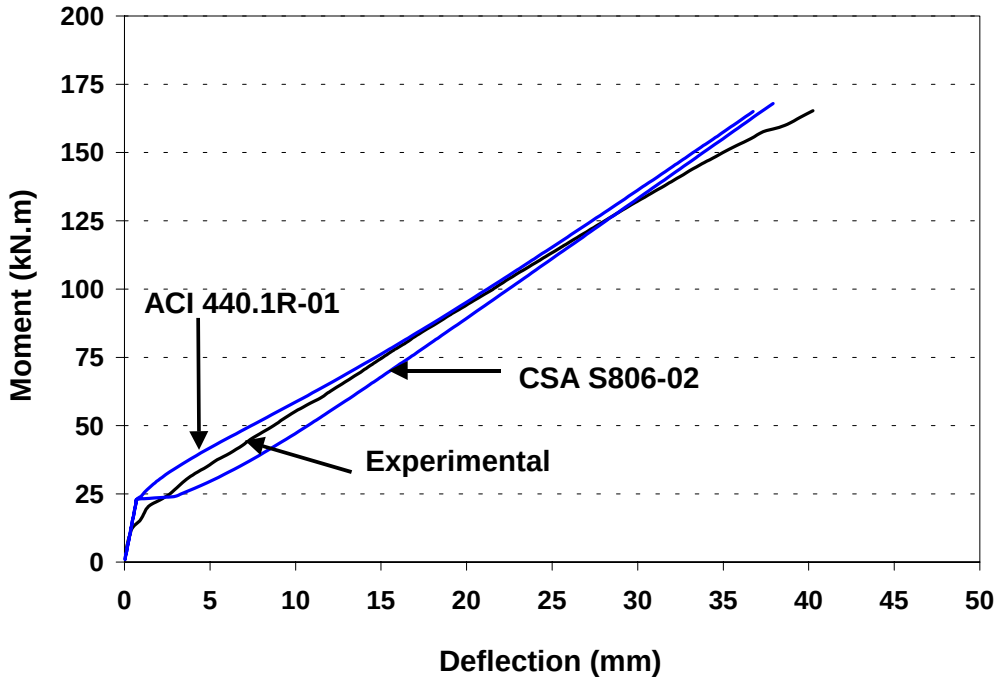

(a) Slab S-C2B

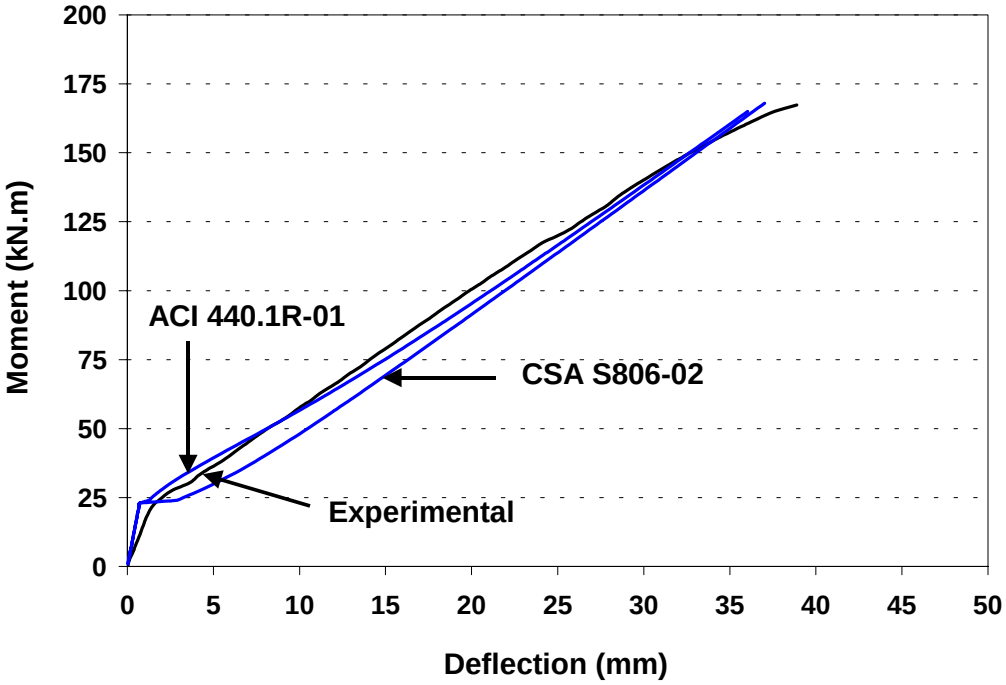

(b) Slab S-G3B

Figure 8. Comparison of test results and codes' predictions

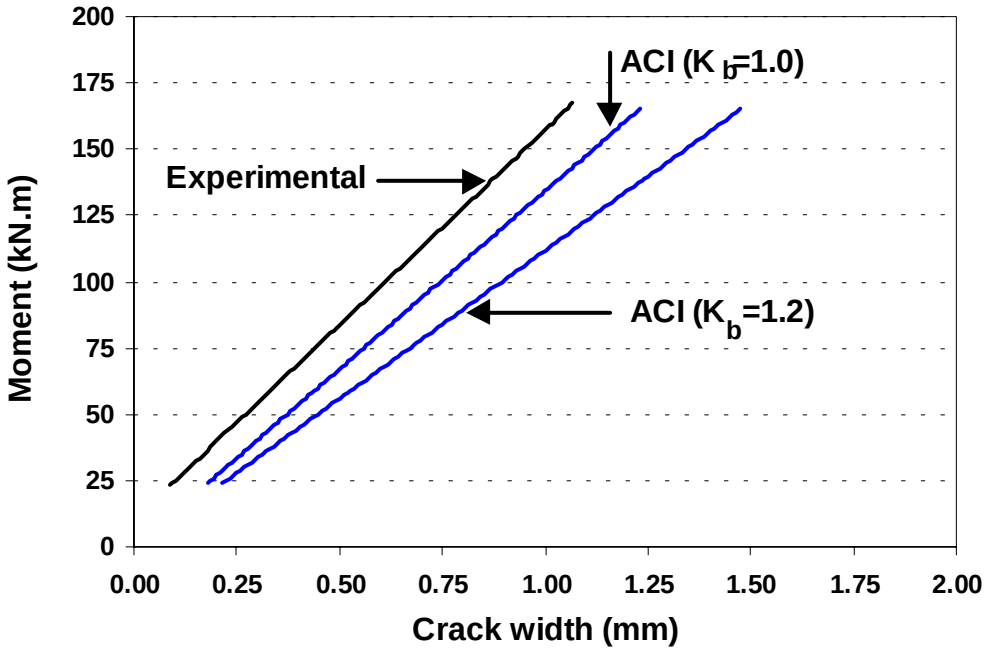

a) Slab S-C2B

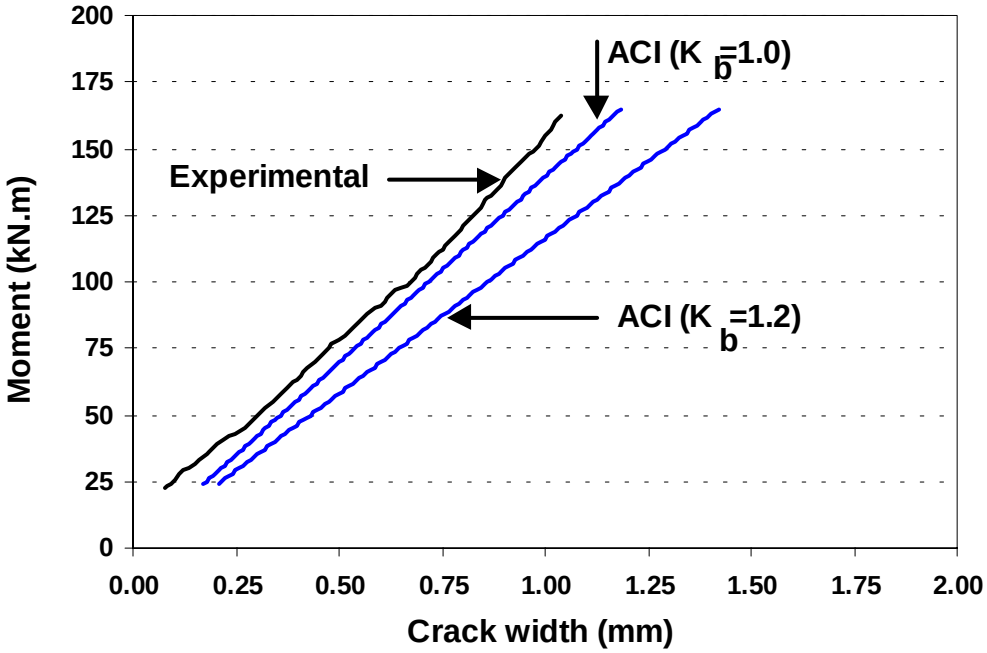

b) Slab S-G3B

Figure 9. Theoretical and experimental load-crack width relationship

APPENDIX A - DESIGN EXAMPLE

Calculations of the Design Moments in Concrete Bridge Deck Slabs
Based on CHBDC (CAN/CSA S6-00)

(1) Geometrical Data

- Slab thickness 200 mm
- Slab is continuous over prestressed concrete girders 5 Girders
- Span of deck slab 2.70 m
- Overhang of 1.35 m
- Top clear concrete cover 60 mm
- Bottom clear concrete cover 38 mm
- Thickness of pavement 65 mm
- Concrete curb 468 × 280 mm

(2) Design Moments in the Deck Slab

Dead Loads and Corresponding Moments

Own weight of the slab $= 0.2 \times 23.5 = 4.7$ kN/m^2

Own weight of pavement $= 0.065 \times 24 = 1.56$ kN/m^2

Service dead load, w_{ds} $= 4.7 + 1.56 = 6.26$ kN/m^2

Factored dead load, w_{du} $= 1.2 \times 4.7 + 1.5 \times 1.56 = 7.98$ kN/m^2

Service moment due to dead load, $M_{ds} = 0.071\ w_{ds}\ l^2 = 0.071 \times 6.26 \times (2.7)^2 = 3.24$ kN.m/m

Factored moment due to dead load, $M_{du} = 0.071\ w_{du}\ l^2 = 0.071 \times 7.98 \times (2.7)^2 = 4.13$ kN.m/m

Live Loads and Corresponding Moments

Transverse moment in the deck slab induced by the wheel load (Art. 5.7.1.7.1, CAN/CSA-S6-00)

The total transverse moment is given by: $M_y = \dfrac{(S + 0.6)P}{10}$

where $S = 2.7$ m, and $P = 87.5$ kN

$$M_y = \frac{(2.7 + 0.6)\ 87.5}{10} = 28.87\ \ kN.m/\text{m}$$

For slab continuous on beams for more than 3 spans and considering the dynamic load allowance of 0.4 (*Art 3.8.4.5.3*), the maximum moment in the deck slab is given by:

Service moment due to wheel load = 0.8 × 28.87 × 1.4 = 32.34 kN.m/m

For transitory loads (*Art 3.5.1*), the load factor L^5 = 1.7

Factored moment due to wheel load = 1.7 × 32.34 = 54.98 kN.m/m

The service design moment = 32.34 + 3.24

= <u>35.58</u> kN.m/m (top and bottom moment)

The factored design moment = 1.7 × 32.34 + 4.13

= <u>59.11</u> kN.m/m (top and bottom moment)

<u>(3) Design Moments at the Overhang</u>

Dead Loads and Corresponding Moments

Concrete curb:	0.468 × 0.28 × 23.5	= 3.08 kN/m
Steel barrier:		= 0.60 kN/m
Concrete slab:	0.2 × 23.5	= 4.7 kN/m^2
Railing supports:	0.065 × 24	= 1.56 kN/m^2

Service moment due to dead load = 3.08 (1.35 - 0.2) + 0.6 (1.35 - 0.15)
+ 4.7 (1.35) ^{2}/2 + 1.56 (1.35 - 0.45)^2/2
= 3.54 + 0.72 + 4.28 + 0.64 = 9.18 kN.m/m

Factored moment due to dead load = 1.2 (3.54 + 4.28) + 1.1 × 0.72 + 1.5 × 0.64
= 11.14 kN.m/m

Live Loads and Corresponding Moments at the Overhang

Transverse moment in the overhang induced by the wheel load (Service Load) (Art. 5.7.1.6.1, CAN/CSA-S6-00)

$$M_y = \frac{2PA}{\pi} \frac{1}{\left[1+\left(\frac{Ax}{C-y}\right)^2\right]^2} \times (1+DMF)$$

x = 0, y = 0, and P = 87.5 kN

A = 0.55 (from Figure 5.7.1.6.1, without edge stiffening, for t_1/t_2 = 1.0, c/s_c = 0.445, y = 0)

DMF = 0.3 (Dynamic modification factor)

$$M_y = \frac{2 \times (87.5) \times (0.55)}{3.14} \times (1 + DMF) \qquad = 39.8 \text{ kN.m/m}$$

The service design moment at the overhang = 39.8 + 9.18 = **48.98** kN.m/m

The factored design moment at the overhang = 1.7 × 39.8 + 11.14 = **78.8** kN.m/m